Journal of Thermal Analysis and Calorimetry
https://doi.org/10.1007/s10973-020-09694-9

Non-axisymmetric three-dimensional stagnation-point flow and heat transfer under a jet impingement boiling

M. R. Mohaghegh[1] · Asghar B. Rahimi[2] · Shohel Mahmud[1]

Received: 10 December 2019 / Accepted: 10 April 2020
© Akadémiai Kiadó, Budapest, Hungary 2020

Abstract

The non-axisymmetric three-dimensional flow and heat transfer in the stagnation-point region of a planar jet impingement boiling on a flat surface has been investigated by using similarity solution approach, considering additional diffusivity terms in momentum and energy equations as a result of bubble-induced mixing in flow. The free jet stream along z direction impinges on the surface and produces a flow with different velocity components. This situation may happen if the flow pattern on the plate is bounded from both sides in one of the directions, because of any physical limitation or due to conditions of the surface such as moving plates or stretching sheets with different values of stretching velocities in the x and y directions. The governing equations have been transformed into ordinary differential equations by introducing appropriate similarity variables, and an exact solution has been obtained for three-dimensional boiling problem for the first time. The similarity variables have been presented based on non-axisymmetric three-dimensional and additional diffusivity effects. The bubble-induced diffusion due to bubble formation, growth, departure and collapse causes an enhancement in heat transfer rate from the surface to the bulk flow. The total heat flux transferred from the surface to the flow has been estimated as summation of the single-phase heat transfer due to forced convection and the nucleate boiling heat flux due to bubble-induced diffusion. The effects of the velocity components ratio and the ratio between the maximum total diffusivity to the molecular diffusivity on the flow field and heat transfer characteristics have been obtained and discussed and illustrated graphically. A comparison of the predicted heat flux has been made with previously published experimental data. As expected, the average deviation values show relatively more accurate results for the three-dimensional simulation than the two-dimensional one because of being closer to the experimental conditions.

Keywords Non-axisymmetric three-dimensional stagnation-point flow · Jet impingement boiling · Nucleate boiling heat transfer · Similarity solution · Bubble-induced mixing

Nomenclature

c_p	Specific heat (J kg^{-1} °C^{-1})
C	Velocity gradient
f	Dimensionless function used in Eq. (10)
g	Dimensionless function used in Eq. (10)
h	Heat transfer coefficient (W m^{-2} °C^{-1})
Ja	Jacob number
k	Thermal conductivity (W m^{-1} °C^{-1})
M	Decay function of the thermal additional diffusivity, defined in Eq. (15)
N	Decay function of the momentum additional diffusivity, defined in Eq. (14)
p	Pressure (N m^{-2})
Pr	Prandtl number
$\mathrm{Pr_t}$	Bubble-induced Prandtl number
q''	Heat flux (W m^{-2})
$\mathrm{Re_j}$	Jet Reynolds number
T	Temperature (°C or K)
ΔT	Temperature difference (°C or K)
u	Velocity component in x direction (m s^{-1})
v	Velocity component y direction (m s^{-1})
V_j	Jet velocity
w	Velocity component in z direction (m s^{-1})
w_j	Jet width (m)
We	Weber number

✉ Asghar B. Rahimi
rahimiab@um.ac.ir

[1] School of Engineering, University of Guelph, Guelph, ON, Canada

[2] Faculty of Engineering, Ferdowsi University of Mashhad, P.O. Box No. 91775-1111, Mashhad, Iran

Published online: 27 April 2020

Greek symbols

α	Molecular thermal diffusivity ($m^2\ s^{-1}$)
ν	Molecular kinematic diffusivity ($m^2\ s^{-1}$)
μ	Molecular dynamic diffusivity ($kg\ ms^{-1}$)
ρ	Density
λ	Velocity components ratio
ε	Additional diffusivity ($m^2\ s^{-1}$)
ε^+	Dimensionless total diffusivity
η	Dimensionless distance from surface
θ	Dimensionless temperature

Subscripts

axi	Axisymmetric
b	Bubble
cr	Critical value
FDB	Fully developed boiling
j	Jet related value
h	Thermal energy
l	Liquid
m	Momentum
max	Maximum value
model	Model-predicted value
nb	Nucleate boiling
s	Surface (wall)
sp	Single phase
sub	Sub-cooled
sup	Superheat
v	Vapor
ε	Related to the bubble-induced diffusivity
w	Related to the jet width
2-D	Two-dimensional value
3-D	Three-dimensional value
∞	Free stream related value

Superscripts

′	First derivative
″	Second derivative

Introduction

The jet impingement boiling mechanism is preferred for cooling processes due to high efficiency in extracting high heat flux accompanied by small increase in wall superheat. Many industrial and engineering applications include cooling processes of hot sheet materials, computer chips and microelectronic circuits, hot rolling steel strip and nuclear power plants that use liquid impinging jets. Hence, the jet impingement cooling has been an interesting problem in studies of the recent decades. The numerous studies have been performed for both single- and two-phase (boiling) conditions. Single-phase impinging jets have been studied extensively, experimentally and numerically, by various researchers, i.e., [1–8] but the two-phase state in which the impinging liquid is allowed to boil on the hot surface is rather less explored analytically and numerically and most studies in this case have been performed experimentally, i.e., [9–19]. Because of the complexity of the jet impingement boiling process, this type of cooling mechanism is still not fully understood. Recently, a mechanistic modeling of two-dimensional jet impingement boiling was reported by the present authors [20, 21]. They presented a modified superposition approach to predict the rate of heat transfer in the stagnation region of a planar jet impingement boiling on a hot flat plate.

The common numerical modeling approach used empirical correlations or constant parameters to fit to the experimental data with not much insight into the underlying physical/analytical conceptions [9, 10, 22–24]. Analytical models have been presented to predict the heat transfer from laminar impinging jets but in single-phase cases [5, 25–27].

A through literature review reveals lots of experimental works and relatively few numerical and analytical studies on jet impingement boiling, especially for the three-dimensional case. However, because of the complex mechanism of the jet impingement boiling, it will be so difficult to develop an analytical model to predict the rate of heat transfer from the surface. On the other hand, the existing numerical models based on computational fluid dynamics (CFD) [28–31] and direct numerical simulation (DNS) [32] of flow boiling are very costly in solving details of the phase change.

Once the surface temperature T_s becomes well above the saturation temperature of the liquid, T_{sat}, isolated vapor bubbles start to nucleate and grow on the surface. So, an enhancement in surface heat flux happens as a result of cyclic nucleation, growth, departure and collapse of vapor bubbles (some bubbles may collapse without departure from the surface [33]). In pool boiling mechanism in which a heated surface submerged in a large volume of stagnant liquid exists, a deep insight into the nucleation sites and bubble dynamics is needed. In flow boiling like what happens during jet impingement boiling, in addition to the bubble dynamics, jet hydrodynamics and the interaction between them have a significant effect on the mechanism of flow and the heat transfer. It makes jet impingement boiling mechanism more complex than pool boiling.

Gunther [33] measured bubble growth rates by a high-speed photography technique. He found that increase in sub-cooling and surface heat flux led to a decrease in mean bubble diameters and an increase in bubble populations and frequencies. Also, he found typical orders of magnitude for lifetimes of 0.1 ms and for maximum radii of 0.1 mm. Also, Timm et al. [34] reported that the typical time and length scales associated with bubble dynamics in boiling flows are in the order of 0.01–0.1 ms and 0.1–1 m, respectively. These results and values show why numerical simulations of boiling heat transfer are computationally expensive. In nucleate

pool boiling, depending on degree of liquid sub-cooling, generated bubbles on the heating surface can be detached from the wall when buoyancy forces exceed inertial and surface tension forces (saturated pool boiling) or collapse due to condensation shortly after formation without leaving the wall (in highly sub-cooled boiling) [33]. In nucleate flow boiling, hydrodynamics of flow has a significant effect on bubble dynamics (formation, growth, departure and collapse), i.e., it may lead to slide of vapor bubbles on the surface with or without bubbles lift off.

Above analysis may lead to propose a mechanistic prediction model of nucleate boiling heat transfer by using additional diffusion conception that adds the effects of bubbles dynamics including bubble growth, departure (slide or liftoff) and collapse in diffusion terms of momentum and energy equations (similar to concept of eddy diffusivity in turbulence flow modeling), without deal with very small length and time scales, mentioned in prior. The concept of bubble-induced diffusion assumes that, in addition to the fluid molecular diffusivity, there is an additional diffusivity due to the bubble-induced mixing in flow. So, this concept can be easily implemented in the conservation equations as a result of advantage of this method and solving the equations analytically or numerically to obtain details of the flow and temperature fields.

The idea of applying additional diffusivity to predict the surface heat flux in jet impingement boiling was first proposed by Timm et al. [34], who presented an analytical model to determine the rate of the heat transfer from a planar free jet impinging on a hot flat surface. They used the diffusion terms in the momentum and energy equations by adding additional diffusivity due to bubble-induced diffusion. They considered the ranges of the surface temperature that cause film boiling regime to occur. Then, Omar et al. [35] developed this idea for nucleate boiling from a planar free jet impinging on a hot flat surface and with a more comprehensive insight to calculate bubble-induced diffusion term due to bubbles nucleation.

In this study, a non-axisymmetric three-dimensional analytical solution of flow and heat transfer in the stagnation region of a planar water jet impingement is presented to predict the surface heat flux in single and nucleate boiling regime, underlying effect of bubble-induced diffusion in bulk flow. The non-axisymmetric three-dimensional nucleate boiling case may happen if the flow pattern on the hot plate is bounded from both sides in one of the directions, because of any physical limitation, like space limitations in power electronics cooling or due to conditions of the surface such as moving plates [36] or stretching sheets with different values of the surface velocities in the x and y directions [26, 37]. Appropriate similarity variables for governing equations are derived for this problem. The obtained ordinary differential equations are solved numerically by using Runge–Kutta fourth-order method. To our knowledge, no attempts have been made to analyze non-axisymmetric three-dimensional jet impingement boiling, analytically or numerically. By the fairly simple approach, presented in this study, two main significant reductions in the complexity and cost of the computations of flow boiling simulations are obtained. The first significant reduction is in modeling of nucleate boiling by concept of bubble-induced diffusion that considers the effect of bubble generation on the flow and the heat transfer rate without the need to solve details of phase change. And the second significant reduction is in simulation of three-dimensional problem that is a big challenge with extensive cost of computation in CFD and DNS simulation, by similarity solution approach.

Modeling of the problem

The two-dimensional flow profile of an impinging planer jet is depicted in Fig. 1. As it can be seen, flow symmetrically is diverted around the stagnation line. The boundary layer thickness is constant in the stagnation region because of the balance between the stream acceleration (thinning boundary layer thickness) and the viscous diffusion (thickening boundary layer thickness) [38].

A non-axisymmetric three-dimensional case of velocity fields in Cartesian coordinates (x, y, z) with corresponding velocity components (u, v, w) is depicted in Fig. 2. The non-axisymmetric three-dimensional case may happen if the flow pattern on the plate is bounded from both sides in one of the directions, because of any physical limitation or due to configurations of the surface such as moving plates or stretching sheets with different values of the surface velocities in the x and y directions. In the axisymmetric case, the velocity components u and v in x and y directions are the same if the ratio of velocity components is unity; $\lambda = 1$.

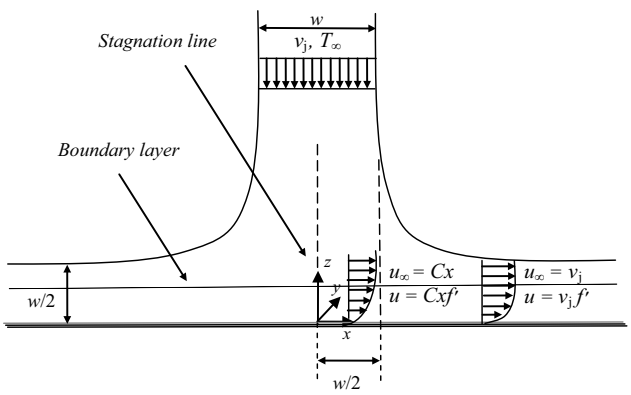

Fig. 1 Stagnation flow profile of an impinging planer jet [21]

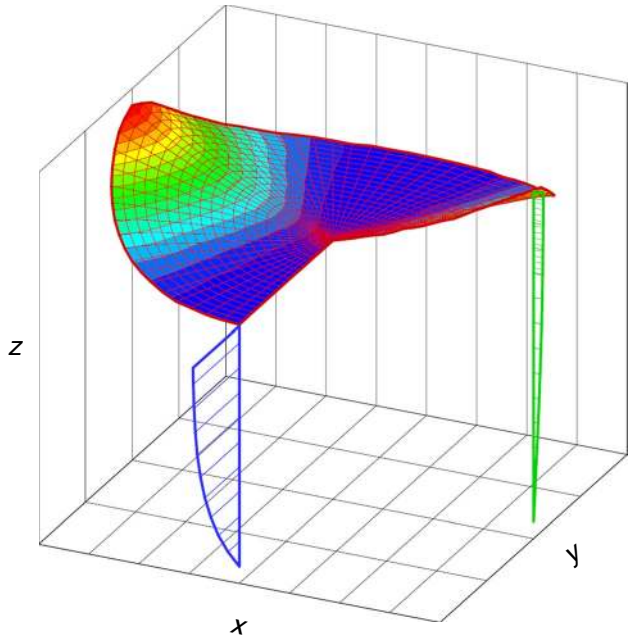

Fig. 2 Three-dimensional stream surface and velocity profiles

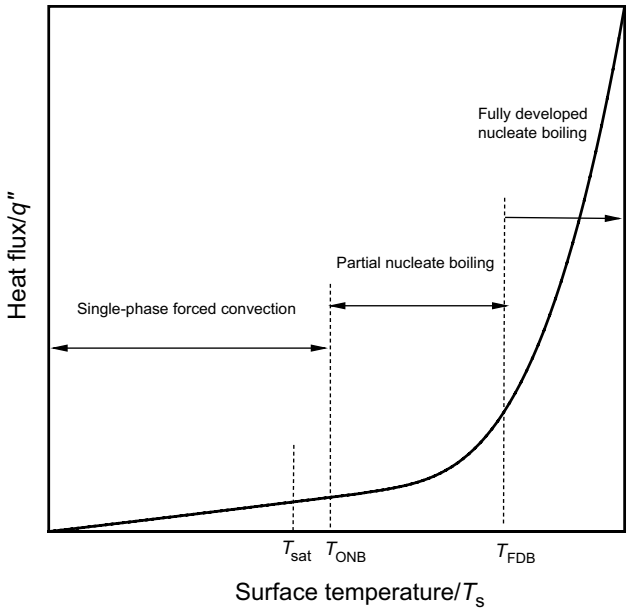

Fig. 3 Schematic of the boiling curve in single and nucleate boiling regimes

When the liquid jet with a given velocity and sub-cooling temperature impinges on the hot surface, various heat transfer regimes can be observed depending on the degree of wall superheat. The variations in the rates of heat transfer (q'') against wall superheat (ΔT_{sat}) for the different heat transfer regimes are plotted on a graph named boiling curve [39]. The boiling curve for three different regimes: forced convection (single phase) and partial and fully developed nucleate boiling (two phase) which are under study in the present paper, is schematically depicted in Fig. 3.

For temperatures less than the surface temperature at the onset of nucleate boiling, T_{ONB}, single-phase heat transfer regime occurs. Once the surface temperature is sufficiently higher than the saturation temperature of the liquid, T_{sat}, the first isolated vapor bubbles start to nucleate and grow on the surface [40]. At this temperature (T_{ONB} in Fig. 3), the regime of partial nucleate boiling begins. This regime is affected by both bulk flow hydrodynamic and bubble dynamic including, formation, growth and collapse of isolated vapor bubbles. The surface heat flux increases as a result of vapor bubbles formation on the surface and bubble-induced mixing in bulk flow. With further increasing the surface temperature, more bubbles are formed on the surface. The rate of heat transfer increases when they grow, slide and depart from the surface, which leads to transition from partial to fully developed nucleate boiling regime.

In nucleate boiling regime on a hot surface, it can be assumed that the surface is covered with these bubbles that form a very thin layer as bubbly layer [35], with thickness of bubble diameter in the adjacent region to the surface. Since bubbles nucleate, grow and depart or collapse cyclically on the surface, additional diffusivity is induced into the bulk flow that will cause to improve the heat transfer from the surface. So, the additional diffusivity as a result of bubble-induced diffusion is added to molecular diffusivity in the diffusion term of the conservation equations. According to the physics of the problem, this additional diffusivity should have maximum value at the wall and decrease and decay away from the surface in an asymptotic manner [34]. The liquid temperature in the bubbly layer is assumed equal to the surface temperature (superheated liquid), and the top of the bubbly layer (lower boundary of the computational domain) is at the saturation temperature (saturated liquid). By increasing wall distance, temperature decreases till it reaches the temperature of the free stream flow (T_∞) in the edge of the boundary layer (upper boundary of the computational domain). So, the boundary layer equations of x and y momentum and energy, presented within the computational domain of interest, are solved by similarity solution approach in order to obtain the velocity and the temperature fields under the effect of bubble-induced diffusions of momentum and energy from the bubbly layer.

Problem formulation

Consider a steady, three-dimensional, incompressible, laminar boundary layer flow and heat transfer of a viscous fluid in the neighborhood of a stagnation point on a flat plate

located in the plane $z = 0$. The problem is formulated in Cartesian coordinates (x, y, z) with corresponding velocity components (u, v, w) under the following assumptions:

- Liquid properties in boundary layer are estimated in film temperature $T_f = \frac{1}{2}(T_s + T_\infty)$.
- Net vapor generation is negligible. Hence, heat transfer due to evaporation is negligible [34, 35].
- The influence of bubble-induced diffusion due to bubbles nucleation is taken into account by additional diffusivity terms (α_m and α_h) in momentum and energy equations.
- The surface temperature in the stagnation region is assumed constant and well above the saturation temperature for nucleate boiling to occur.
- The fluid temperature at the lower boundary of the computational domain is at saturation temperature.
- Temperature distribution within the superheated bubbly layer near the wall is not considered.
- Boundary layer flow is assumed laminar. For stagnation flow, critical Reynolds number ($\mathrm{Re}_{w,cr} = \frac{v_j w}{\nu}$) was reported about 4000 by Lienhard [1]. The range of Reynolds number in the present study (with $v_j \le 1.25$ and $w_j = 1$ mm) is less than 4000.

The three-dimensional boundary layer equations are presented as follows:

Continuity

$$\frac{\partial u}{\partial x} + \frac{\partial v}{\partial y} + \frac{\partial w}{\partial z} = 0 \tag{1}$$

Momentum

$$u\frac{\partial u}{\partial x} + v\frac{\partial u}{\partial y} + w\frac{\partial u}{\partial z} = -\frac{1}{\rho_l}\frac{\partial p}{\partial x} + \frac{\partial}{\partial x}\left[(\varepsilon_m + \nu)\frac{\partial u}{\partial x}\right] + \frac{\partial}{\partial y}\left[(\varepsilon_m + \nu)\frac{\partial u}{\partial y}\right] + \frac{\partial}{\partial z}\left[(\varepsilon_m + \nu)\frac{\partial u}{\partial z}\right] \tag{2}$$

$$u\frac{\partial v}{\partial x} + v\frac{\partial v}{\partial y} + w\frac{\partial v}{\partial z} = -\frac{1}{\rho_l}\frac{\partial p}{\partial y} + \frac{\partial}{\partial x}\left[(\varepsilon_m + \nu)\frac{\partial v}{\partial x}\right] + \frac{\partial}{\partial y}\left[(\varepsilon_m + \nu)\frac{\partial v}{\partial y}\right] + \frac{\partial}{\partial z}\left[(\varepsilon_m + \nu)\frac{\partial v}{\partial z}\right] \tag{3}$$

Energy

$$u\frac{\partial T}{\partial x} + v\frac{\partial T}{\partial y} + w\frac{\partial T}{\partial z} = \frac{\partial}{\partial x}\left[(\varepsilon_h + \alpha)\frac{\partial T}{\partial x}\right] + \frac{\partial}{\partial y}\left[(\varepsilon_h + \alpha)\frac{\partial T}{\partial y}\right] + \frac{\partial}{\partial z}\left[(\varepsilon_h + \alpha)\frac{\partial T}{\partial z}\right] \tag{4}$$

Employing the Bernoulli's equation in the potential region, the following relations between free stream velocity $U(x)$ and $V(y)$, and the pressure gradients in x and y directions are specified, respectively:

$$-\frac{1}{\rho}\frac{\partial p}{\partial x} = U\frac{\mathrm{d}U}{\mathrm{d}x} \tag{5}$$

$$-\frac{1}{\rho}\frac{\partial p}{\partial y} = V\frac{\mathrm{d}V}{\mathrm{d}y} \tag{6}$$

The velocity components of the classical potential flow solution are as follows [26]:

$$U = C\lambda x \tag{7}$$

$$V = Cy \tag{8}$$

$$W = -C(\lambda + 1)z \tag{9}$$

where $0 < \lambda \le 1$ is presented as ratio of velocity component u to velocity component v which indicates the difference between the velocity components in x and y directions. For $\lambda = 1$, free-stream velocity components in x and y directions are the same. So, the problem will be converted into an axisymmetric problem with no differences between the flow characteristics in x and y directions. The C parameter introduces the velocity gradient that is expressed in terms of the jet velocity and the jet width as $C = \bar{C}\frac{v_j}{w}$, [41] where the value of $\bar{C} = \frac{\pi}{4}$ [25, 41].

Similarity solution

To convert partial differential Eqs. (1)–(4) into a set of ordinary differential equations, the following dimensionless similarity variables are introduced:

$$\eta = \sqrt{\frac{C}{\varepsilon_{max}}}z$$
$$u = C\lambda x f'(\eta),\ v = Cy\left[f'(\eta) + g'(\eta)\right],$$
$$w = -\sqrt{C\varepsilon_{max}}\left[g(\eta) + (\lambda + 1)f(\eta)\right],$$
$$\theta(\eta) = \frac{T - T_\infty}{T_{sat} - T_\infty} \tag{10}$$

where ε_{max} is maximum total diffusivity defined as $\varepsilon_{max} = \varepsilon_{m_{max}} + \nu$.

Substituting these transformations into momentum and energy Eqs. (2) through (4) yields the following nonlinear ordinary differential equations:

$$Nf''' + \left[N' + g + (\lambda + 1)f\right]f'' + \lambda(1 - f'^2) = 0 \tag{11}$$

$$Ng''' + \left[N' + g + (\lambda + 1)f\right]g'' - \left(g' + 2f'\right)g' + (1 - \lambda)\left(1 - f'^2\right) = 0 \tag{12}$$

$$M\theta'' + \left[M' + g + (\lambda + 1)f\right]\theta' = 0 \tag{13}$$

where N and M functions are defined as:

$$N(\eta) = \frac{\varepsilon_m + \nu}{\varepsilon_{max}} \tag{14}$$

$$M(\eta) = \frac{\varepsilon_h + \alpha}{\varepsilon_{max}} \tag{15}$$

The boundary conditions in Eqs. (11), (12) and (13) are as:

$$\eta = 0 \ : \ \begin{cases} u = 0,\ v = 0,\ w = 0,\ T = T_{sat} \\ f' = f = 0,\ g' = g = 0,\ \theta = 1 \end{cases} \tag{16}$$

$$\eta \to \infty \ : \ \begin{cases} u = U,\ v = V,\ T = T_{\infty} \\ f' = 1,\ g' = 0,\ \theta = 0 \end{cases} \tag{17}$$

The expression of the ratio of additional diffusivity $\varepsilon_m/\varepsilon_{max}$ as a function of dimensionless distance in boundary layer,η, should satisfy the behavior of bubble-induced diffusion into the bulk flow in order to have maximum value on the lower surface (the bubbly layer), and to decay by distancing from the surface. So, it has been assumed in the following form [34]:

$$\frac{\varepsilon_m}{\varepsilon_{max}} = e^{-c_\varepsilon \eta} \tag{18}$$

where c_ε is equal to two. By substituting Eq. (18) into Eq. (14), N function can be defined as:

$$N(\eta) = e^{-c_\varepsilon \eta} + \frac{1}{\varepsilon^+} \tag{19}$$

where ε^+ is the ratio between the maximum total diffusivity and the molecular diffusivity (dimensionless total diffusivity):

$$\varepsilon^+ = \frac{\varepsilon_{max}}{\nu} \tag{20}$$

Considering Eqs. (14), (15) and (20), molecular Prandtl number, $\mathrm{Pr} = \frac{\nu}{\alpha}$, and bubble-induced diffusion Prandtl number, $\mathrm{Pr_t} = \frac{\varepsilon_\nu}{\varepsilon_h}$, dimensionless function M can be derived in terms of N, Pr and $\mathrm{Pr_t}$ as the following form:

$$M(\eta) = \frac{N(\eta)}{\mathrm{Pr_t}} + \frac{1}{\varepsilon^+}\left(\frac{1}{\mathrm{Pr}} - \frac{1}{\mathrm{Pr_t}}\right) \tag{21}$$

Substituting Eq. (19) into Eq. (13) yields the following form for energy equation:

$$\left[N + \frac{1}{\varepsilon^+}\left(\frac{\mathrm{Pr_t}}{\mathrm{Pr}} - 1\right)\right]\theta'' + \left[N' + \mathrm{Pr_t}\,(g + (\lambda + 1)f)\right]\theta' = 0 \tag{22}$$

For $\lambda = 1$, the problem is converted into an axisymmetric with no differences between the flow characteristics in x and y directions.

Note, for boiling flows ($\varepsilon_m, \varepsilon_h \succ 0$) ε^+ is always larger than unity, Eq. (20). With no boiling, no additional diffusion exists, $\varepsilon_m = \varepsilon_h = 0$, so $\varepsilon_{max} = \nu$ and hence considering Eqs. (14), (15) and (20)$\varepsilon^+ = 1$, $N = 1$, $M = \mathrm{Pr}^{-1}$, $N' = M = 0$. So, similarity parameters Eq. (10) and ODEs (11)–(13) are reduced to a single-phase case as the following:

$$f_{sp}''' + \left[g_{sp} + (\lambda + 1)f_{sp}\right]f_{sp}'' + \lambda(1 - f_{sp}'^2) = 0 \tag{23}$$

$$g_{sp}''' + \left[g_{sp} + (\lambda + 1)f_{sp}\right]g_{sp}'' - \left(g_{sp}' + 2f_{sp}'\right)g_{sp}' + (1 - \lambda)\left(1 - f_{sp}'^2\right) = 0 \tag{24}$$

$$\theta_{sp}'' + \mathrm{Pr}\left[g_{sp} + (\lambda + 1)f_{sp}\right]\theta_{sp}' = 0 \tag{25}$$

where dimensionless temperature function for single-phase case is defined based on surface temperature T_s as a lower boundary condition of the computational domain:

$$\theta_{sp}(\eta) = \frac{T - T_{\infty}}{T_s - T_{\infty}} \tag{26}$$

Also, for the two-dimensional case, the governing equations are obtained as follows:

$$Nf''' + \left[N' + f\right]f'' + 1 - f'^2 = 0 \tag{27}$$

$$\left[N + \frac{1}{\varepsilon^+}\left(\frac{\mathrm{Pr_t}}{\mathrm{Pr}} - 1\right)\right]\theta'' + \left[N' + \mathrm{Pr_t} f\right]\theta' = 0 \tag{28}$$

In this study, the additional diffusivities in the momentum and in the energy equations are assumed equal [34, 35]. Hence, the bubble-induced diffusion Prandtl number is $\mathrm{Pr_t} = 1$.

Timm et al. [34] and Omar et al. [35] obtained energy equation of the two-dimensional case for the same problem, in the following form:

$$N\theta'' + \left[N' + f\right]\theta' = 0 \tag{29}$$

A comparison between the obtained equations of Refs. [34, 35], Eq. (29), with derived ODE form of the two-dimensional equations in this study, Eq. (28), shows error in ODE form of the obtained energy equation of Refs [34, 35]., even under condition $\mathrm{Pr_t} = 1$. Equation (28) (also Eq. (22) for three-dimensional case) shows energy equation is a function of Prandtl number (as for single-phase case [26, 38]) which is in accordance with physics of the problem. But Eq. (29) does not reflect this effect and for larger Prandtl numbers, like in high sub-cooled liquid jets, could be a source of error.

Some of the numerical results, obtained from three-dimensional and for two-dimensional solution for presented problem, have been presented and discussed in the next section.

Results and discussion

Equations (11), (12) and (13) with the boundary conditions (16) and (17) are a set of highly nonlinear ordinary differential equations with boundary values. One of the most convenient and efficient method to solve boundary value problems of a set of nonlinear ODEs is the fourth-order Runge–Kutta numerical method. Equations (11)–(13) are a set of boundary value problems with an unknown parameter in upper boundary condition (η_∞). So, the upper boundary conditions $f'(\infty)$, $g'(\infty)$ and $\theta(\infty)$ may be substituted by the initial boundary conditions $f''(0)$, $g''(0)$ and $\theta'(0)$, to convert boundary value problem to an initial value problem. For this purpose, the shooting technique is applied along with the fourth-order Runge–Kutta method with initial guesses for values of $f''(0)$, $g''(0)$ and $\theta'(0)$, and an iterative solution procedure till satisfying the upper boundary conditions $f'(\infty) = 1$, $g'(\infty) = 0$ and $\theta(\infty) = 0$.

The solution algorithm to obtain the nucleate boiling heat flux q''_{nb} is shown in Fig. 4 as a flowchart.

Equations (11)–(13) depend on two parameters λ and ε^+. First, the effect of λ is investigated on the velocity and temperature fields, for a typical $\varepsilon^+ = 10$. Then, effect of ε^+ will be investigated.

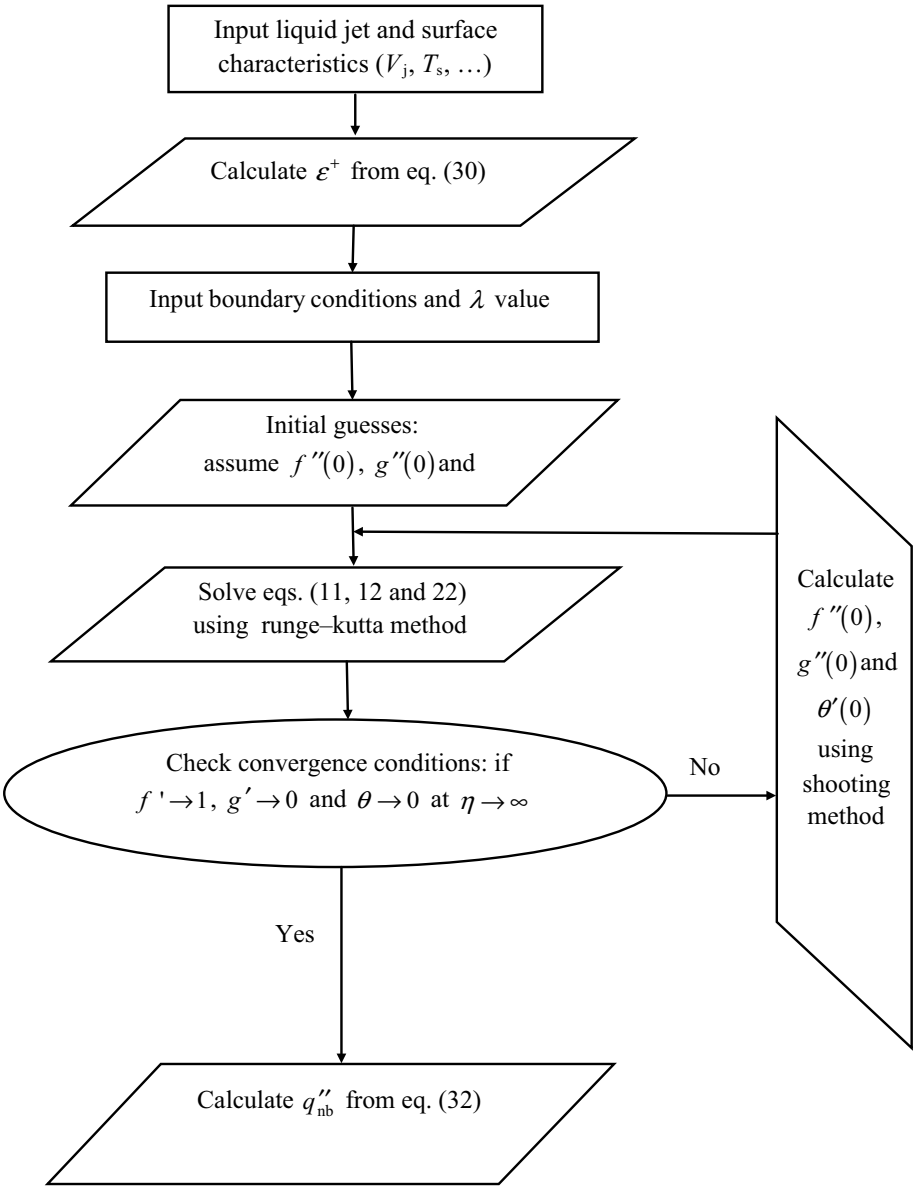

Fig. 4 The flowchart for numerical procedure

Table 1 presents dimensionless coefficients of shear stress in x and y directions and dimensionless coefficients of heat flux transferred to the bulk flow as a result of the enhanced bubble-induced diffusion that are functions of initial boundary conditions obtained from a convergence solution of Eqs. (11)–(13).

Comparison of the results in every column of Table 1 reveals this important point that the shear-stress coefficient in both x and y directions and the heat transfer coefficient in the vicinity of the plate increase by increasing in λ and are the largest for the axisymmetric case ($\lambda = 1$). It is because of increase in gradients of velocity and temperature, as a result of a decrease in the thermal and velocity boundary layer thickness. This can also be observed from Fig. 5a–d, too. These figures show the effect of velocity ratio λ on dimensionless velocity profiles proportional to velocity components u and v, profiles of g and g', and dimensionless temperature profiles θ, for $\varepsilon^+ = 10$. Note the numerical solution showed that dimensionless boundary layer thickness η_∞ is in order of (about) 5 for a wide range of different values of λ and ε^+, and also the numerical solution showed the results with not significant variations in solution for $\eta \succ 3$. So, the presented figures in this study have been illustrated just till $\eta = 3$ to show the variations of dimensionless velocity and temperature profiles in boundary layer.

It is also noted that when λ increases, the variation of the profiles shows validation of the non-axisymmetric case compared to the axisymmetric one, again. This result is shown clearer in Fig. 5c where variations of functions of g and g' (contribution of being non-axisymmetric) in boundary layer is shown for different values of λ. As it can be seen, the smaller λ leads to the larger g and g', and therefore, the difference between the velocity components becomes larger. When $\lambda \to 1$, contribution of non-axisymmetric is reduced; hence, $g' \to 0$ and $g \to 0$, and the two velocity components (u, v) become the same which validates the presented result compared to the axisymmetric problem case. Exact equality of the coefficients of the shear stress in x and y directions (Table 1, columns 2 and 3, last row) validates the result again.

The dimensionless total diffusivity ε^+ is a function of fluid properties, jet velocity, liquid sub-cooling and wall superheat. Omar et al. [35] correlated ε^+ as a function of dimensionless groups (Re_b, We_b, Ja_{sup} and Ja_{sub}) in the following form:

$$\varepsilon^+ = \frac{Re_b^{x_1} Ja_{sup}^{x_4} Ja_{sup}^{x_5}}{We_b^{x_2} + x_3} \tag{30}$$

where $x_1 = -0.7736$, $x_2 = 4.283$, $x_3 = 5.634$, $x_4 = 4.167$ and $x_5 = -1.586$. Equation (30) reflects the effect of liquid jet properties and surface conditions on the value of additional diffusivity due to bubble-induced mixing. For example, according to Eq. (30), increasing the jet velocity or increasing the degree of sub-cooling would result in a lower diffusivity which is consistent with what is expected from the physics of the jet impingement boiling. Because the mentioned effects cause a decrease in bubbles diameter and number of active bubble nucleation sites [32, 33, 35, 42]. Even more increase in the jet velocity or the degree of sub-cooling can lead to a delay in the onset of nucleate boiling (ONB) as a result of a delay in bubbles formation and nucleation [10, 40]. On the contrary, an increase in the degree of wall superheat is represented by Ja_{sup}; hence, higher additional diffusivity causes the bubbles to nucleate at a larger diameter and higher number [32, 33, 43].

To investigate the effect of ε^+ on the velocity and temperature fields, the dimensionless profiles f' and θ of an axisymmetric case $\lambda = 1$ (therefore $u = v$ and $g = g' = 0$) are depicted, for different values of ε^+ in Fig. 6a, b, respectively. As it is shown, significant effect of ε^+ on the velocity and temperature fields does not occur for $\varepsilon^+ \geq 10$. Since variation of velocity and temperature on the lower boundary of computational domain is proportional to shear stress and heat transfer rate, these variations are listed in Table 2. It is evident from this table that coefficients of shear stress and heat transfer rate are almost not dependent on ε^+ for values of $\varepsilon^+ \geq 10$. This is why the previous result where the effects of λ were investigated was presented for $\varepsilon^+ = 10$ and is enough reliable for higher ε^+. Since an increase in ε^+ shows the stronger effect of bubble-induced diffusion in bulk flow, the higher ε^+ is related to the fully developed boiling regime in boiling curve (Fig. 1), while the smaller values are related to the partial boiling regime. Comparisons of the results in columns related to axisymmetric and two-dimensional cases show that the shear stress and the heat transfer for axisymmetric case are a little larger than the ones for the two-dimensional case in all ranges of ε^+, as expected, because the thermal and velocity boundary layers in the two-dimensional case are thicker than in the axisymmetric one.

By determining the value of the coefficient of heat transfer at the lower boundary of the computational domain, $\theta'(0)$, the rate of the heat flux transferred to the bulk flow as

Table 1 The shear-stress coefficients in x direction $\lambda f''(0)$, y direction $f''(0) + g''(0)$ and heat transfer coefficient on the wall $\theta'(0)$, for $\varepsilon^+ = 10$

λ	$\lambda f''(0)$	$f''(0) + g''(0)$	$\theta'(0)$
0.25	0.124617	0.871817	−0.34027
0.5	0.328127	0.886873	−0.37625
0.75	0.597567	0.904633	−0.41443
1	0.924154	0.924154	−0.45305

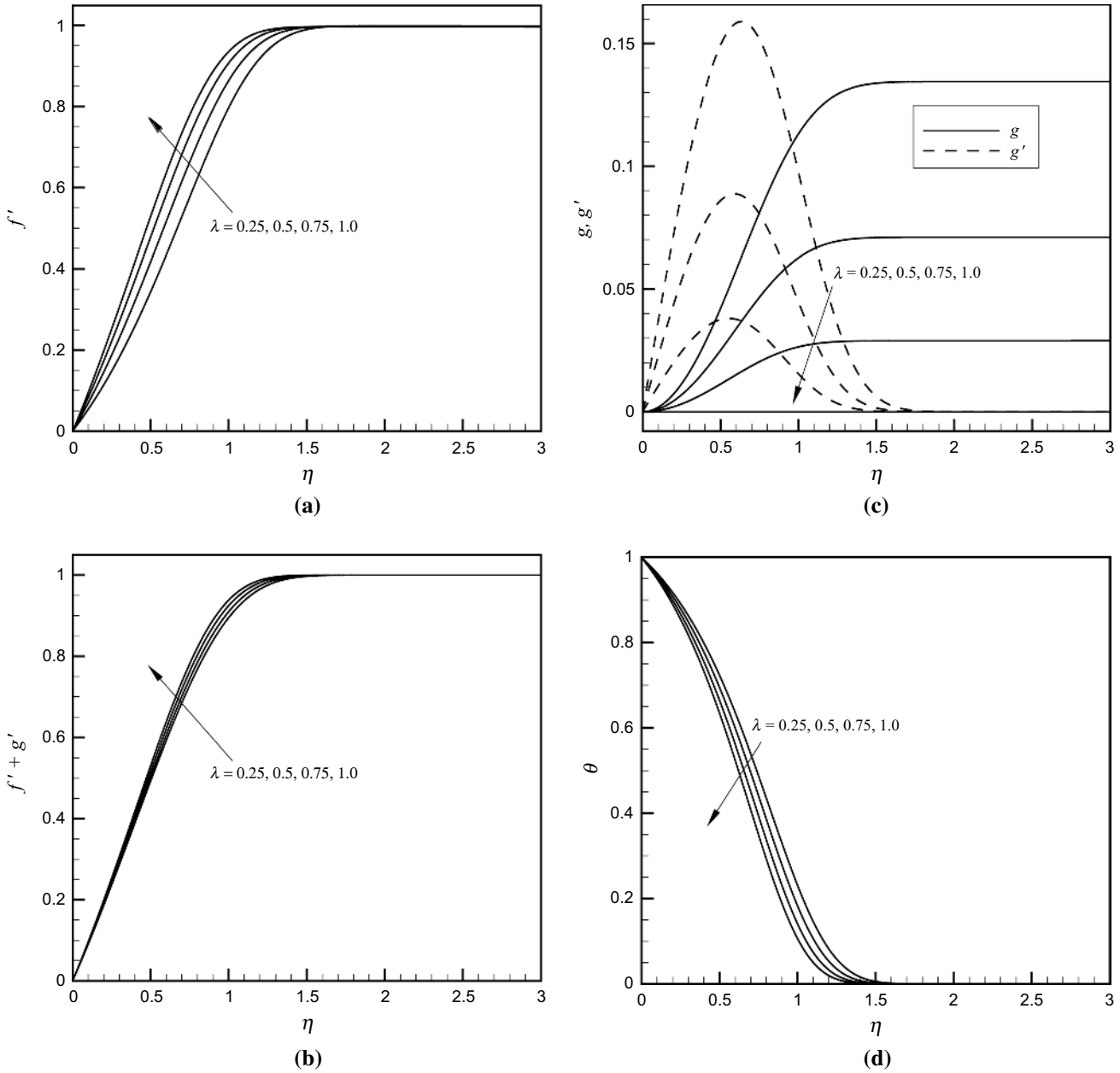

Fig. 5 Effect of velocity ratio λ on dimensionless profiles: **a** u velocity component, f', **b** i velocity component $f' + g'$, **c** g, g' and **d** temperature θ

a result of the bubble-induced diffusion can be obtained by the following equation:

$$q''_{\mathrm{nb}} = \rho_{\mathrm{l}} c_{\mathrm{p}} \varepsilon_{\max} \left.\frac{\partial T}{\partial z}\right|_{\mathrm{y}=0} = \rho_{\mathrm{l}} c_{\mathrm{p}} \Delta T_{\mathrm{sub}} \sqrt{C \varepsilon_{\max}} \left.\frac{\mathrm{d}\theta}{\mathrm{d}\eta}\right|_{\eta=0} \tag{31}$$

In the above equation, the effect of the liquid properties and sub-cooling ΔT_{sub} on the boiling heat flux has been shown, explicitly. The effects of the jet velocity v_{j} and the wall superheat ΔT_{sup} on the boiling heat flux have been taken into account by the values of $\varepsilon_{\max}$ and temperature gradient at the bubbly layer, $\left.\frac{\mathrm{d}\theta}{\mathrm{d}\eta}\right|_{\eta=0}$. By substituting Eq. (20) into Eq. (31), nucleate boiling heat flux q''_{nb} can be rewritten as a function of the dimensionless total diffusivity ε^{+}:

$$q''_{\mathrm{nb}} = \varepsilon^{+0.5} \rho_{\mathrm{l}} c_{\mathrm{p}} \Delta T_{\mathrm{sub}} \sqrt{C\nu} \left.\frac{\mathrm{d}\theta}{\mathrm{d}\eta}\right|_{\eta=0} \tag{32}$$

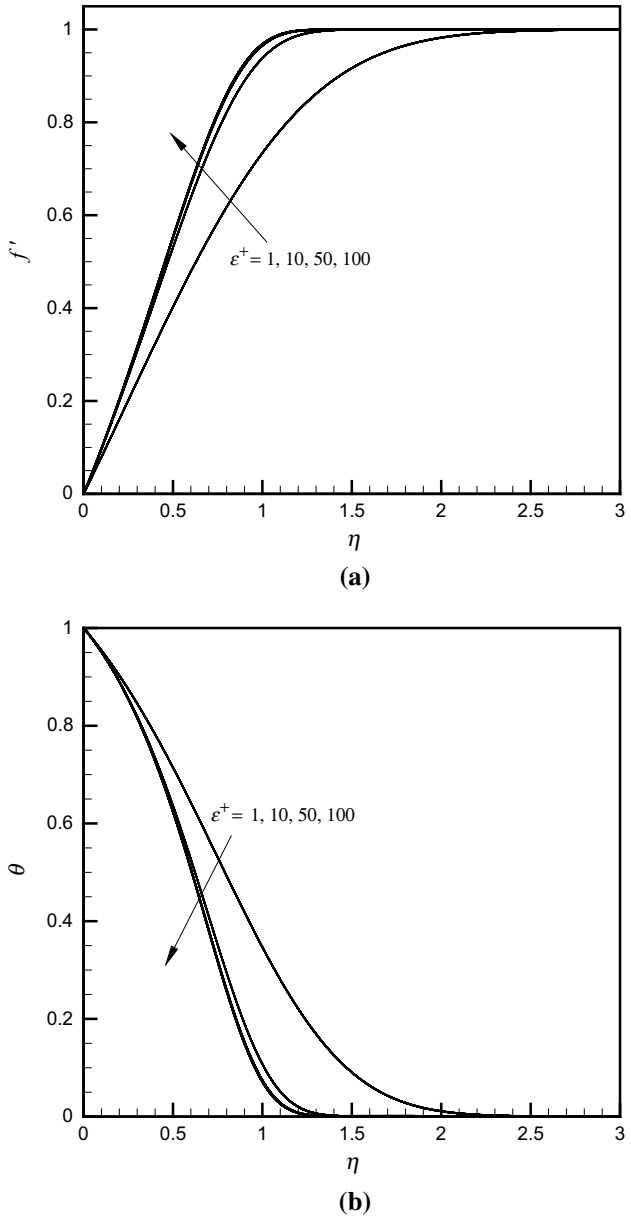

Fig. 6 Effect of dimensionless total diffusivity ε^+ on dimensionless profiles: **a** u velocity component, f', **b** temperature θ

Table 2 The shear-stress coefficients in x direction $\lambda f''(0)$ and y direction $f''(0) + g''(0)$ and heat transfer coefficient on the wall $\theta'(0)$, for different values of ε^+

ε^+	$f''(0)$ (3-D$_{axi.}$; $\lambda = 1$)	$f''(0)$ (2-D)	$\theta'(0)$ (3-D$_{axi.}$; $\lambda = 1$)	$\theta'(0)$ (2-D)
1	0.781881	0.732691	−0.42974	−0.3104
2	0.856687	0.801192	−0.44518	−0.31503
4	0.898995	0.838984	−0.45095	−0.31346
6	0.913162	0.851266	−0.45228	−0.31189
8	0.920087	0.857142	−0.4528	−0.31083
10	0.924154	0.860539	−0.45305	−0.31011
50	0.936462	0.870429	−0.45357	−0.30725
100	0.937896	0.871525	−0.4536	−0.30683
200	0.938602	0.871882	−0.45361	−0.30661

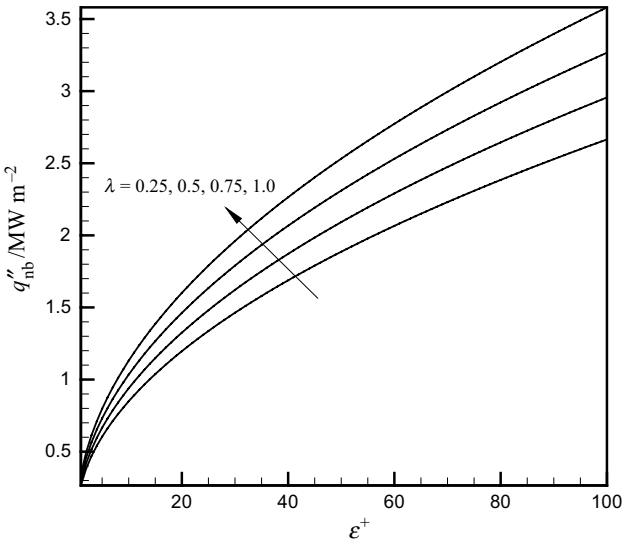

Fig. 7 The variation of q''_{nb}, with respect to ε^+, at different values of λ

The variation of typical values of the nucleate boiling heat flux due to the bubble-induced diffusion q''_{nb} with respect to dimensionless total diffusivity ε^+ is shown in Fig. 7, for different values of λ. As it is expected from the results in Table 1, it is concluded again that the heat transfer coefficient increases by increasing in λ and is the largest value for the axisymmetric case ($\lambda = 1$), in all ranges of ε^+. Also, a comparison of the obtained total heat flux q'', in two-dimensional and axisymmetric cases, has been made and is illustrated in Fig. 8. This validates the results in Table 3 again, which shows that the heat transfer for axisymmetric case is a little larger than the two-dimensional case in all ranges of ε^+. Furthermore, an increase in ε^+ means stronger effect of bubble-induced diffusion in bulk flow. Hence, as it is expected,

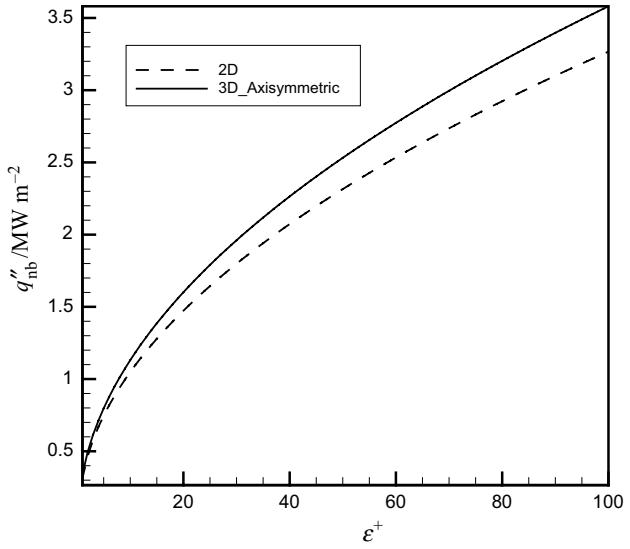

Fig. 8 The variation of q''_{nb}, with respect to ε^+, for two-dimensional and axisymmetric cases

with increasing ε^+, the heat transfer rate also increases. The higher ε^+ is related to the fully developed boiling regime, and the smaller ones are related to the partial boiling regime.

The total heat flux transferred from the surface into the flow is estimated by adding contribution of the nucleate boiling due to bubble-induced mixing, calculated from Eq. (32), to the contribution of single-phase heat transfer due to forced convection. The single-phase heat transfer can be calculated by the following relation:

$$q''_{sp} = -\rho_l c_p \alpha \left.\frac{\partial T}{\partial z}\right|_{y=0} = -\rho_l c_p \overset{-1}{\Pr} \Delta T_s \sqrt{C\nu} \left.\frac{d\theta_{sp}}{d\eta}\right|_{\eta=0} \tag{33}$$

So, the total heat flux is calculated as the following:

$$q''_{model} = q''_{sp} + q''_{nb} = -\rho_l c_p \sqrt{C\nu}\left[\overset{-1}{\Pr} \Delta T_s \theta'_{sp}(0) + \varepsilon^{+0.5} \Delta T_{sub} \theta'(0)\right] \tag{34}$$

To validate the results of the present study, the obtained results are compared with the experimental data of Ref. [35] and are listed in Table 3 as well as in Fig. 9. In Fig. 9, it is shown that the predicted results are in reasonable agreement with the experimental results, in both two-dimensional (2-D) and non-axisymmetric three-dimensional (3-D) cases for the different jet (velocity and temperature) and surface conditions (surface temperature).

The rectangular nozzle, used by Ref. [35], is in size of 1 mm and 8 mm in the x and y directions, respectively; hence,λ has a value of 0.125. According to Table 3, the overall variation of the predicted values with the experimental data is in the range of 35 to −3.5% for the two-dimensional case and in the range of −32 to 0.5% for the three-dimensional case. The results show that values of the relative error for the three-dimensional simulation are a little less than the two-dimensional one, for all test cases. To make a better comparison between the obtained results of the two-dimensional and three-dimensional simulations, an average error analysis has been made as the following:

$$\overline{\text{Error}} = \frac{1}{n}\sum_{i=1}^{n}\left|\frac{q''_{i,model} - q''_{i,exp}}{q''_{i,exp}}\right| \tag{35}$$

This analysis shows that the average deviation of the experimental data is 19% for the two-dimensional simulation and 15.7% for the non-axisymmetric three-dimensional simulation. This comparative analysis of average error shows relatively more accurate results for the non-axisymmetric three-dimensional simulation than the two-dimensional simulation as a result of a being closer to the experimental conditions.

Table 3 The comparison between the predicted total heat fluxes from hot surface q''(MW m^{-2}), obtained from two-dimensional and non-axisymmetric three-dimensional simulations, and experimental data [35]

v_j/m s^{-1}	ΔT_{sub}/°C	ΔT_{sup}/°C	ε^+	q''_{exp} [35]	$q''_{model,2-D}$	Relative error	$q''_{model,3-D}$	Relative error
0.4	21	12.5	10.89	1.53	1.38	−10.06	1.43	−6.32
0.75	10	10.5	8.5	1.17	0.92	−21.19	0.96	−18.01
0.75	15	20	38.2	3.22	2.25	−30.09	2.35	−27.11
0.75	28	19.7	27.5	4.9	3.48	−29.00	3.63	−25.95
0.95	10	17	21	1.8	1.49	−17.42	1.55	−14.00
0.95	10	25	53.3	3.3	2.15	−34.99	2.24	−32.25
0.95	15	11	12.7	1.74	1.63	−6.44	1.70	−2.55
0.95	22	15.5	10.5	2.87	2.25	−21.65	2.34	−18.42
0.95	28	14.5	7.62	2.6	2.51	−3.50	2.61	0.45
1.25	15	7.7	1.36	1.22	1.01	−17.19	1.05	−14.11
1.25	15	22	19.9	2.93	2.42	−17.33	2.52	−13.90

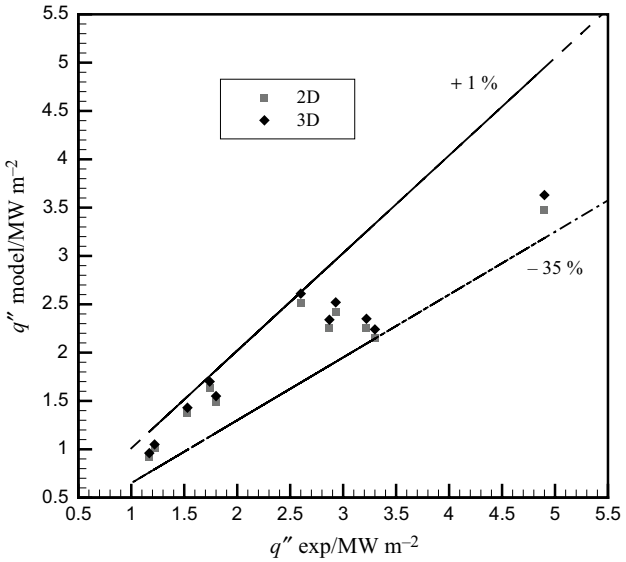

Fig. 9 Model predictions of the total heat flux against experimental data

Conclusions

Modeling of a non-axisymmetric three-dimensional jet impingement boiling which is a significant challenge in heat transfer problems has been done analytically and numerically in this study. The three-dimensional case may occur in flow boiling pattern on a hot plate which is bounded from both sides in one of the directions because of any physical limitation. A non-axisymmetric three-dimensional analytical solution of the flow and heat transfer in the stagnation region of a planar water jet impingement has been presented in this study to predict the surface heat flux in single and nucleate boiling regime, underlying bubble-induced diffusion conception due to bubble formation, growth, departure (slide or liftoff), and collapse on the hot surface, by using similarity solution approach. By this fairly simple approach, two main significant reductions in the complexity and cost of the computations of flow boiling simulations have been accomplished. The first significant reduction is in the modeling of nucleate boiling by concept of bubble-induced diffusion that considers the effect of bubble generation on the flow and the heat transfer rate without the need to solve details of the phase change. And the second significant reduction is the simulation of a three-dimensional problem using similarity solution approach which is much less expensive and time-consuming than the costly computations in CFD and DNS simulations.

The results of the presented analytical solution have shown that the shear-stress coefficient in both directions and the heat transfer coefficient in the vicinity of the plate increase by increasing in λ and has been the largest for the axisymmetric case which are the result of a decrease in the thermal and velocity boundary layer thicknesses. It has also been shown that these coefficients are larger in the axisymmetric case than in the two-dimensional one. It has been deduced that for a fixed value of λ the coefficients of the shear stress and the heat transfer rate are almost independent from ε^+ for values of $\varepsilon^+ \geq 10$.

The obtained results from the present study have been validated using some experimental data. The predicted heat flux has shown a reasonable accuracy with an average deviation of 19% for the two-dimensional case and 15.7% for the non-axisymmetric three-dimensional one that shows a relatively more accurate result for non-axisymmetric three-dimensional simulation than the two-dimensional simulation as a result of a being closer to the experimental conditions.

It has been deduced that the energy equation used in Refs. [34, 35], in the contrary to the energy equation used in our study which is in terms of Prandtl number, could have a source of error for higher Prandtl numbers like i.e., in sub-cooled liquid jets since it does not reflect the effect of this parameter on the temperature field. It has also been reasoned that the dimensionless total diffusivity ε^+ correlated by Omar et al. [35] in Eq. (30) is limited to experimental data in nucleate boiling regime. This can be re-correlated by using a wider range of jet properties (velocity and sub-cooling) and wall superheat in order to cover the through boiling curve including nucleate, transition and film boiling underlying bubble-induced diffusion conception to predict heat flux in all of the mentioned boiling regimes and also to calculate critical heat flux, CHF (as a one of the most interesting and challenging characteristics in the flow boiling) which is the subject of interest of our future work.

Acknowledgements Hereby, the financial support of Ferdowsi University of Mashhad under contract No. 2/47377 is acknowledged during accomplishment of this research.

References

1. Lienhard J. Liquid jet impingement. Ann Rev Heat Transf. 1995;6(6):199–270.
2. Wolf DH, Viskanta R, Incropera FP. Turbulence dissipation in a free-surface jet of water and its effect on local impingement heat transfer from a heated surface: part 2—local heat transfer. J Heat Transf. 1995;117(1):95–103. https://doi.org/10.1115/1.2822330.
3. Zuckerman N, Lior N. Impingement heat transfer: correlations and numerical modeling. J Heat Transf. 2005;127(5):544–52. https://doi.org/10.1115/1.1861921.
4. Abbasi AS, Rahimi AB, Niazmand H. Exact solution of three-dimensional unsteady stagnation flow on a heated plate. J Thermophys Heat Transf. 2011;25:55–8.
5. Abbassi AS, Rahimi AB. Investigation of two-dimensional unsteady stagnation-point flow and heat transfer impinging on an

accelerated flat plate. J Heat Transf. 2012;134(6):064501. https://doi.org/10.1115/1.4005742.
6. Wang B, Guo X, Xie Q, Wang Z, Wang G. Heat transfer characteristic research during jet impinging on top/bottom hot steel plate. Int J Heat Mass Transf. 2016;101:844–51.
7. Hadipour A, Rajabi Zargarabadi M, Dehghan M. Effect of micro-pin characteristics on flow and heat transfer by a circular jet impinging to the flat surface. J Therm Anal Calorim. 2020. https://doi.org/10.1007/s10973-019-09232-2.
8. Matheswaran MM, Arjunan TV, Somasundaram D. Analytical investigation of exergetic performance on jet impingement solar air heater with multiple arc protrusion obstacles. J Therm Anal Calorim. 2019;137(1):253–66. https://doi.org/10.1007/s10973-018-7926-z.
9. Miyasaka Y, Inada S. The effect of pure forced convection on the boiling heat transfer between a two-dimensional subcooled water jet and a heated surface. J Chem Eng Jpn. 1980;13(1):22–8. https://doi.org/10.1252/jcej.13.22.
10. Wolf D, Incropera F, Viskanta R. Jet impingement boiling. Adv Heat Transf. 1993;23:1–132.
11. Wolf D, Incropera F, Viskanta R. Local jet impingement boiling heat transfer. Int J Heat Mass Transf. 1996;39(7):1395–406.
12. Hall DE, Incropera FP, Viskanta R. Jet impingement boiling from a circular free-surface jet during quenching: part 2—two-phase jet. J Heat Transf. 2001;123(5):911–7.
13. Robidou H, Auracher H, Gardin P, Lebouche M, Bogdanić L. Local heat transfer from a hot plate to a water jet. Heat Mass Transf. 2003;39(10):861–7.
14. Karwa N, Gambaryan-Roisman T, Stephan P, Tropea C. Experimental investigation of circular free-surface jet impingement quenching: transient hydrodynamics and heat transfer. Exp Thermal Fluid Sci. 2011;35(7):1435–43.
15. Li Y-Y, Liu Z-H, Wang Q. Experimental study on critical heat flux of steady boiling for high-velocity slot jet impinging on the stagnation zone. Int J Heat Mass Transf. 2014;70:1–9.
16. Modak M, Nirgude V, Sharma AK, Sahu SK. Experimental study on heat transfer characteristics of circular jet impingement boiling on the variety of structured copper surfaces in stagnation zone. Int J Heat Mass Transf. 2016;50053:V005T15A48. https://doi.org/10.1115/icone24-60682.
17. Karimi Kerdabadi J, Haghanimanesh M, Karimipour A, Toghraie D, Tlili I. The experimental/numerical investigation of variations in strip speed, water shower pattern and water temperature on high-temperature strip cooling rate in hot strip mill. J Therm Anal Calorim. 2020. https://doi.org/10.1007/s10973-019-09052-4.
18. Shafee A, Rezaeianjouybari B, Sheikholeslami M, Allahyari M, Babazadeh H. Boiling process with incorporating nanoparticles through a flattened channel using experimental approach. J Therm Anal Calorim. 2020. https://doi.org/10.1007/s10973-020-09327-1.
19. Sheikholeslami M, Rezaeianjouybari B, Darzi M, Shafee A, Li Z, Nguyen TK. Application of nano-refrigerant for boiling heat transfer enhancement employing an experimental study. Int J Heat Mass Transf. 2019;141:974–80. https://doi.org/10.1016/j.ijheatmasstransfer.2019.07.043.
20. Mohaghegh MR, Rahimi AB. Modeling of nucleate boiling heat transfer of a stagnation-point flow impinging on a hot surface. Thermal Sci. 2019;23(2 Part A):695–706.
21. Mohaghegh MR, Rahimi AB. Single- and two-phase water jet impingement heat transfer on a hot moving surface. J Therm Anal Calorim. 2019;137(4):1401–11. https://doi.org/10.1007/s10973-019-08072-4.
22. Copeland RJ. Boiling heat transfer to a water jet impinging on a flat surface. Ph.D. Thesis. Southern Methodist University, Dallasm, TX; 1970.
23. Ishigai S, Nakanishi S, Ochi T, editors. Boiling heat transfer for a plane water jet impinging on a hot surface. In: Proceedings of the 6th international heat transfer conference: Washington, DC: Hemisphere Publishing Corp; 1978.
24. Miyasaka Y, Inada S, Owase Y. Critical heat flux and subcooled nucleate boiling in transient region between a two-dimensional water jet and a heated surface. J Chem Eng Jpn. 1980;13(1):29–35. https://doi.org/10.1252/jcej.13.29.
25. Zumbrunnen DA. Convective heat and mass transfer in the stagnation region of a laminar planar jet impinging on a moving surface. J Heat Transf. 1991;113(3):563–70. https://doi.org/10.1115/1.2910603.
26. Mohaghegh MR, Rahimi AB. Three-dimensional stagnation-point flow and heat transfer of a dusty fluid toward a stretching sheet. J Heat Transf. 2016;138(11):112001–12. https://doi.org/10.1115/1.4033614.
27. Hsiao K-L. Micropolar nanofluid flow with MHD and viscous dissipation effects towards a stretching sheet with multimedia feature. Int J Heat Mass Transf. 2017;112:983–90. https://doi.org/10.1016/j.ijheatmasstransfer.2017.05.042.
28. Narumanchi S, Troshko A, Bharathan D, Hassani V. Numerical simulations of nucleate boiling in impinging jets: applications in power electronics cooling. Int J Heat Mass Transf. 2008;51(1):1–12.
29. Paul S, Udo F. Simulation of the impinging liquid jet cooling process of a flat plate. Int J Numer Methods Heat Fluid Flow. 2015;25(1):153–70. https://doi.org/10.1108/HFF-04-2013-0151.
30. Shademan M. CFD simulation of impinging jet flows and boiling heat transfer. Ph.D. Thesis. University of Windsor, Canada; 2015.
31. Ramezanzadeh H, Ramiar A, Yousefifard M, Ghasemian M. Numerical analysis of sinusoidal and step pulse velocity effects on an impinging jet quenching process. J Therm Anal Calorim. 2019. https://doi.org/10.1007/s10973-019-08828-y.
32. Dhir VK, Abarajith HS, Li D. Bubble dynamics and heat transfer during pool and flow boiling. Heat Transf Eng. 2007;28(7):608–24. https://doi.org/10.1080/01457630701266421.
33. Gunther FC. Photographic study of surface-boiling heat transfer to water with forced convection. Trans ASME. 1951;73(2):115–23.
34. Timm W, Weinzierl K, Leipertz A. Heat transfer in subcooled jet impingement boiling at high wall temperatures. Int J Heat Mass Transf. 2003;46(8):1385–93.
35. Omar A, Hamed M, Shoukri M. Modeling of nucleate boiling heat transfer under an impinging free jet. Int J Heat Mass Transf. 2009;52(23):5557–66.
36. Ja'fari M, Rahimi AB. Axisymmetric stagnation-point flow and heat transfer of a viscous fluid on a moving plate with time-dependent axial velocity and uniform transpiration. Sci Iran. 2013;20(1):152–61. https://doi.org/10.1016/j.scient.2012.12.010.
37. Tzirtzilakis EE, Kafoussias NG. Three-dimensional magnetic fluid boundary layer flow over a linearly stretching sheet. J Heat Transf. 2009;132(1):011702–8. https://doi.org/10.1115/1.3194765.
38. White FM. Viscous fluid flow. 3rd ed. New York: McGraw-Hill; 2006.
39. Collier JG, Thome JR. Convective boiling and condensation. 3rd ed. Oxford: Clarendon Press; 1994.
40. Hsu YY. On the size range of active nucleation cavities on a heating surface. J Heat Transf. 1962;84(3):207–13. https://doi.org/10.1115/1.3684339.

41. Inada S, Miyasaka Y, Izumi R. A study on the laminar-flow heat transfer between a two-dimensional water jet and a flat surface with constant heat flux. Bull JSME. 1981;24(196):1803–10. https://doi.org/10.1299/jsme1958.24.1803.
42. Omar AM. Experimental study and modeling of nucleate boiling during free planar liquid jet impingement. Hamilton, ON: McMaster University; 2010.
43. Basu N, Warrier GR, Dhir VK. Wall heat flux partitioning during subcooled flow boiling: part II—model validation. J Heat Transf. 2005;127(2):141–8. https://doi.org/10.1115/1.1842785.

Publisher's Note Springer Nature remains neutral with regard to jurisdictional claims in published maps and institutional affiliations.